Evaluation of the 29-km Eta Model. Part II: Subjective Verification over Florida

JOHN MANOBIANCO AND PAUL A. NUTTER*

ENSCO, Inc., Cocoa Beach, Florida, and Applied Meteorology Unit, NASA/Kennedy Space Center, Florida

(Manuscript received 30 March 1998, in final form 15 September 1998)

ABSTRACT

This paper describes a subjective evaluation of the National Centers for Environmental Prediction 29-km (Meso) Eta Model during the 1996 warm (May–August) and cool (October–January) seasons. The companion paper by Nutter and Manobianco presents results from an objective evaluation of the Meso Eta Model at three selected locations during the 1996 and 1997 warm and cool seasons. The overall evaluation is designed to assess the utility of the model for operational weather forecasting by the U.S. Air Force 45th Weather Squadron, National Weather Service (NWS) Spaceflight Meteorology Group, and NWS Office in Melbourne, Florida. In the subjective verification, limited case studies are used to highlight model capabilities and limitations in forecasting convective activity, the location and movement of cold fronts, and the onset of sea breezes over regions including east-central Florida. In addition, contingency tables and categorical scores are used to verify the occurrence of these phenomena throughout the season.

Results from the subjective verification demonstrate that model forecasts of developing weather events such as thunderstorms, sea breezes, and cold fronts are not always as accurate as might otherwise be implied by the seasonally averaged error statistics. Although the objective statistics do not indicate whether the model provides more accurate forecast guidance on average during either the warm or cool seasons, results from the subjective verification suggest that model forecasts over central Florida may be more *useful* during the cool season. This is because the Meso Eta Model resolution is not yet sufficient to resolve the small-scale details of sea and river/lake breeze circulations, thunderstorm outflow boundaries, and other phenomena, which play a dominant role in determining the short-term evolution of weather over east-central Florida during the warm season. Lessons learned from the subjective portion of the Meso Eta evaluation should apply equally as well to the recently upgraded ''early'' Eta Model running with a similar 32-km horizontal resolution.

1. Introduction

The primary mesoscale modeling efforts at the National Centers for Environmental Prediction (NCEP) are focused on the development of the Eta Model (Rogers et al. 1995). By the turn of the century, the Eta Model is projected to be running at a horizontal resolution on the order of 10 km over the entire United States (Kalnay et al. 1996). As part of ongoing efforts to improve the accuracy and utility of forecast products, NCEP continues to update the configuration, initialization, and physical parameterizations of the Eta Model. As numerical models such as the Eta are run at finer horizontal and vertical resolutions and initialized with mesoscale data [e.g., Weather Surveillance Radar-1988D (WSR-88D) radial winds], they have the potential to provide more precise and detailed forecast guidance (Cortinas and Stensrud 1995).

The evaluation of the 29-km version of the Eta Model described here and in the companion paper by Nutter and Manobianco (1999, hereafter referred to as NM99) is designed to assess the utility of the model for weather forecasting in support of operational requirements for the U.S. Air Force 45th Weather Squadron (45WS), National Weather Service (NWS) Spaceflight Meteorology Group (SMG), and NWS Weather Forecast Office in Melbourne, Florida (MLB). The 45WS provides weather support for all ground and launch operations from the Cape Canaveral Air Station/Kennedy Space Center (CCAS/KSC), general aviation at Patrick Air Force Base, and space shuttle ferry flights (Boyd et al. 1995; Priselac et al. 1997). The NWS SMG provides weather forecasts and briefings for all shuttle landings and potential landings and serves as the staff weather office for the Johnson Space Center (Brody et al. 1997). While 45WS and SMG concentrate on direct weather support to the U.S. space program, the NWS MLB provides weather forecasts and warnings of hazardous weather for east-central Florida (Friday 1994).

The 29-km (Meso) Eta Model evaluation was performed by the National Aeronautics and Space Admin-

* Current affiliation: School of Meteorology, University of Oklahoma, Norman, Oklahoma.

Corresponding author address: John Manobianco, ENSCO, Inc., 1980 N. Atlantic Ave., Suite 230, Cocoa Beach, FL 32931.
E-mail: johnm@fl.ensco.com

istration's Applied Meteorology Unit (AMU). The mission of the AMU is to evaluate and transition new technology, tools, and techniques into the real-time operational weather support environment for the 45WS, SMG, and NWS MLB (Ernst and Merceret 1995). Previously, the AMU evaluated a version of the Mesoscale Atmospheric Simulation System (MASS) running locally on a high performance workstation (Manobianco et al. 1996). The motivation for running mesoscale modeling systems like MASS locally at KSC/CCAS is to provide detailed short-range (<24 h) guidance for forecasts of winds, clouds, and severe weather such as thunderstorms. However, many components of the MASS evaluation indicated that it could not consistently produce more skillful short-range precipitation and wind forecasts than those already provided by NCEP's Nested Grid Model (Manobianco 1996). The limitations with MASS were likely due to a number of factors including but not limited to insufficient horizontal resolution, deficiencies in the physical parameterizations, and lack of initialization data to specify accurate mesoscale distributions of atmospheric moisture, temperature, winds, and moisture in the soil and surface cover layer (Manobianco 1996). Until the aforementioned deficiencies with resolution, physics, and initialization of local mesoscale models are remedied, AMU efforts on mesoscale modeling have been redirected toward evaluating the forecast utility provided by NCEP's Meso Eta Model.

The Meso Eta Model evaluation utilizes both objective and subjective methodologies. The companion paper (NM99) presents results from the AMU's objective evaluation at CCAS (XMR), Florida; Edwards Air Force Base (EDW), California; and Tampa Bay (TBW), Florida. The objective verification focuses on the overall accuracy of Meso Eta Model point forecasts of wind, temperature, and moisture at XMR, EDW, and TBW for the 1996 and 1997 warm (May–August) and cool seasons (September–January). Statistics presented by NM99 demonstrate that although forecasts of selected parameters at these three stations contain identifiable biases that vary by season and location, they do have the capability to provide useful forecast guidance as long as users recognize possible sources for the errors. However, the objective verification is limited to the sensible characteristics of different weather events that are transitory in both space and time. The statistical results alone therefore do not indicate whether the model provides enhanced utility in forecasting the extent, timing, motion, or intensity of individual weather events.

Subjective verification is thus chosen to quantify the added value provided by model forecasts for specific phenomena. The subjective or phenomenological verification presented here is designed to assess the Eta Model's capabilities and limitations in forecasting convective activity, the location and movement of cold fronts, and the onset of sea breezes over regions including east-central Florida. These phenomena are selected due to their importance for evaluating launch commit criteria for manned and unmanned vehicle launches and flight rules for shuttle landings. In addition, severe weather associated with thunderstorms can be hazardous to the general public and to equipment and personnel performing ground operations at KSC/CCAS.

TABLE 1. Observed and forecast 2-m temperatures (°C) and temperature difference (ΔT) between MCO and buoy 41009 for 7–8 June 1996. Forecast values are shown in parentheses.

Time (UTC)/Date	Orlando International Airport (MCO)	Buoy 41009	ΔT (MCO-41009)
1500/7 Jun	29.4 (27.3)	26.7 (26.0)	2.7 (1.3)
1800/7 Jun	32.8 (30.8)	26.7 (26.5)	6.1 (4.3)
2100/7 Jun	33.3 (31.7)	26.7 (26.9)	6.6 (4.8)
0000/8 Jun	28.9 (27.8)	26.7 (26.5)	2.2 (1.3)

The objective of this paper is to describe the AMU's subjective component of the Meso Eta Model evaluation over Florida. The paper is organized as follows. Section 2 provides a very brief overview of the Eta Model and describes the evaluation protocol. Sections 3, 4, and 5 present limited analyses from selected case studies and seasonal verification of sea breezes, thunderstorms, and cold fronts, respectively. Section 5 contains a summary and conclusions.

2. Model and evaluation overview

This section begins with a brief overview of the Eta Model and then describes the protocol and data used for the subjective components of the Meso Eta Model evaluation. The overall model evaluation described here and in NM99 is specifically focused on determining the capabilities, limitations, and utility of the 29-km Eta Model to support operational weather forecasting at 45WS, SMG, and NWS MLB. For this reason, the subjective evaluation strategy was determined by a group of potential model users consisting of several meteorologists and forecasters from 45WS, SMG, and NWS MLB.

a. Eta Model overview

The 80-km, 38-layer version of the Eta Model replaced the Limited-Area Fine Mesh Model in June 1993 (Black 1994). In October 1995, NCEP improved the horizontal resolution of the operational ''early'' Eta Model from 80 to 48 km. In August 1995, NCEP began running an operational mesoscale version of the Eta Model with a horizontal resolution of 29 km and 50 vertical layers (Mesinger 1996). The relevant numerics and physics of the Eta Model are summarized by NM99 in their Table 1.

The Eta Data Assimilation System (EDAS) for the ''early'' 48-km Eta consists of four 3-h analysis–forecast cycles that incorporate high-frequency observations

such as aircraft and profiler data (Rogers et al. 1996). The Meso Eta is also initialized with the EDAS but it runs for one 3-h analysis–forecast cycle from 0000 to 0300 UTC or 1200 to 1500 UTC. The EDAS begins with a first guess from the Global Data Assimilation System (GDAS). NCEP has implemented several changes to the Eta Model initialization procedures since the AMU completed the Meso Eta subjective evaluation described in this paper. In October 1997, the EDAS began assimilating all available total precipitable water from *Geostationary Operational Environmental Satellites-8/9* (*GOES-8/9*) sounders (CIMSS 1997). On 9 February 1998, NCEP began running an upgraded, 32-km version of the ''early'' Eta Model using three-dimensional variational analysis and ''partial'' continuous EDAS where soil, cloud, and turbulent kinetic energy parameters are cycled from the previous model analysis and first-guess variables are obtained from GDAS (Rogers et al. 1997; EMC 1998). More specific details regarding the dynamics, physics, data assimilation, and other aspects of the Eta Model configuration are provided elsewhere (Black 1994; Rogers et al. 1995; Rogers et al. 1996; Zhao et al. 1997).

b. Subjective evaluation protocol and data

One aspect of the subjective evaluation consisted of daily, real-time warm season forecast exercises by AMU personnel using the Meso Eta Model. The daily weather forecast discussion was held on weekdays during the warm season evaluation period (May–August 1996) at approximately 1330 UTC (0930 EDT). In part, this component of the subjective evaluation was designed to simulate how operational forecasters may visualize, interpret, and use the 0300 UTC cycle of the Meso Eta Model to assist in forecasting the onset of the East and/or West Coast sea breeze and the occurrence of convection within the vicinity of XMR.

A second aspect of the subjective evaluation consisted of limited analyses from selected case studies and seasonal verification of sea breezes, thunderstorms, and cold fronts. This component of the evaluation was designed to assess the added value provided by the Meso Eta Model in forecasting these phenomena. Seasonal verification for sea breezes and thunderstorms included all days during the warm season when both observational and forecast data are available. A similar procedure was followed for the verification of cold fronts using data collected during the cool season.

Forecast and observational data used for the daily forecast exercises, selected case studies, and seasonal verification were collected and archived by the AMU in real time. The 29-km Eta data were obtained via the Internet from the National Oceanic and Atmospheric Administration's Information Center (NIC) ftp server.[1] NCEP interpolates the 29-km Eta gridded model output to the Advanced Weather Interactive Processing System (AWIPS) 40-km grid at 3-h intervals for the entire 33-h Meso Eta forecast period. The AWIPS 40-km gridded fields from the 0300 UTC cycle of the Meso Eta were downloaded at approximately 0900 UTC. Since gridded fields from the 1500 UTC cycle are not available in time to provide early morning guidance in forecasting afternoon sea breezes and thunderstorms, they were not examined as part of this evaluation. Observational data were also archived daily in order to perform the case study analyses and seasonal verifications. These data included surface, KSC/CCAS mesonet towers, rawinsonde, KSC/CCAS 915-MHz Doppler radar wind profiler, and *GOES-8* visible and infrared (IR) satellite data. Although data from the Melbourne WSR-88D were not archived by the AMU for case studies or seasonal verification, these data were used in real time during the warm season forecast exercises to verify the onset of the east coast sea breeze and convection within the vicinity of XMR.

3. Sea-breeze verification

The sea/land breeze is a well-documented mesoscale circulation that affects many coastal areas of the world including the peninsula of Florida (Pielke and Segal 1986). Numerous observational (e.g., Blanchard and Lopez 1985) and numerical (e.g., Pielke 1974; Boybeyi and Raman 1992) studies have demonstrated how the timing and location of convection across Florida is often modulated by local interactions between the sea-breeze circulation and prevailing synoptic-scale wind. For this reason, it is useful to compare characteristics of the observed sea breeze with those forecast by the Meso Eta Model. With its 29-km gridpoint spacing, the model's horizontal resolution is too coarse to resolve the detailed, mesoscale structure of sea breezes (cf. Atkins and Wakimoto 1997) that are common along the Florida coastlines during the warm season. Nevertheless, the model can forecast certain characteristics of the observed sea breeze including a thermally direct circulation that results from differential low-level heating across the land–sea interface. The verification consists of both a case study and statistics that show how reliably the model can forecast the occurrence of the sea breeze over Florida during the warm season from May through August 1996.

a. Case example

The example presented here is an analysis of forecast and observed sea-breeze development over the Florida peninsula on 7 June 1996. This case is chosen because it illustrates the typical 29-km Eta Model signature of the sea breeze that is often forecast during the warm season. Another reason for selecting 7 June is the availability of both model and observational data needed for

[1] At the time of writing, forecast point and grid data could be obtained via anonymous ftp from the NIC Web site (nic.fb4.noaa.gov).

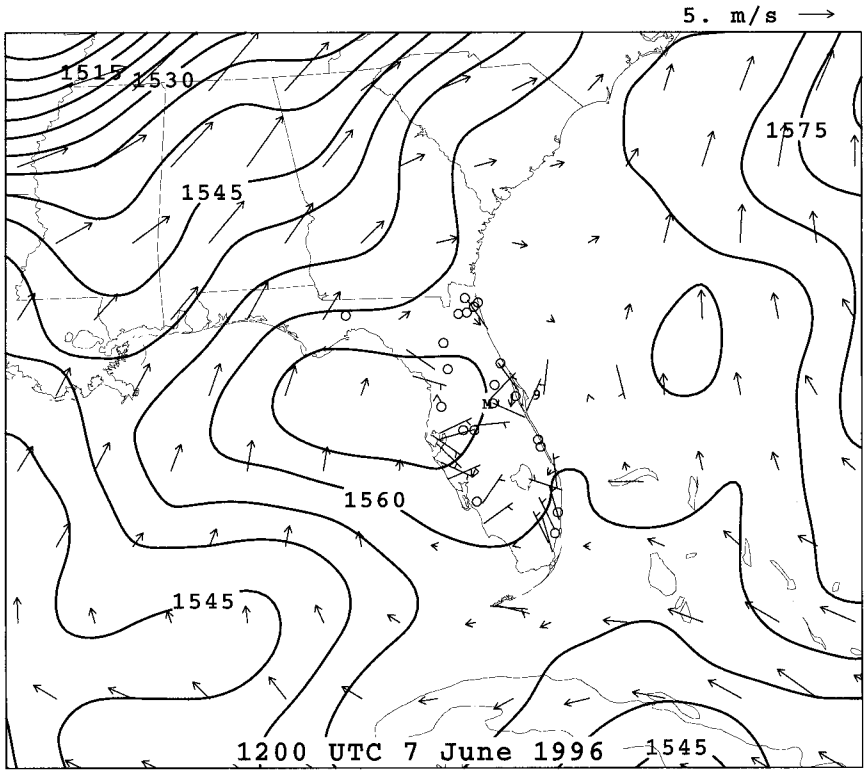

FIG. 1. Synoptic overview from 0-h forecast of the 48-km Eta Model run initialized at 1200 UTC 7 Jun 1996. The 850-mb geopotential heights (m) contoured every 5 m are shown by thick solid lines. Vectors represent the 950–650-mb-layer averaged winds. The vector length is proportional to wind speed with a representative 5 m s^{-1} vector shown in the upper-right corner of the figure. The station locations for Orlando International Airport (MCO) and buoy 41009 are given by the ''M'' and ''9'' symbols, respectively. Observed surface winds from standard land and buoy sites at 1200 UTC are plotted as wind barbs (short barb = 2.5 m s^{-1}, long barb = 5 m s^{-1}). Open circle denotes calm wind.

the analysis. The following sections present observations of the sea breeze followed by an examination of the Meso Eta forecast to distinguish clearly the model capabilities and limitations in depicting the structure and evolution of the sea-breeze circulation.

1) OBSERVATIONS

A limited synoptic overview of the large-scale conditions at 1200 UTC 7 June 1996 is shown in Fig. 1. This analysis is obtained from the 0-h forecast of the 48-km Eta Model run initialized at 1200 UTC 7 June 1996. At that time, the Florida peninsula is under the influence of a ridge axis oriented west-to-east across the central portion of the state (Fig. 1) and a closed high in the eastern Gulf of Mexico, as shown by the 850-mb geopotential heights in Fig. 1. The 950–650-mb-layer averaged wind vectors reveal that lower-tropospheric winds are light (2.5 m s^{-1}) and variable over Florida in association with weak geopotential height gradients. Observed surface winds along the east and west coasts of Florida are also light and variable with offshore components along sections of both coasts (Fig. 1).

A peninsula-scale perspective of the sea breeze along Florida's east and west coasts is shown by the 1-km GOES visible imagery and observed surface winds from standard Aviation Routine Weather Report (METAR) and buoy stations (Fig. 2). The development and movement of the sea breeze can be approximated from the location of narrow bands of shallow cumulus clouds, shifts in wind direction from offshore to onshore flow, and/or increases in wind speed along either coast. It is important to point out that sea-breeze circulations are likely present before their signatures appear as bands of visible clouds (Weckwerth et al. 1997). In addition, shallow cumulus cloud bands can be obscured by thunderstorm anvil debris or other high-level clouds. However, these limitations are not critical for the case presented here since the visible imagery is used in conjunction with surface observations to illustrate the qualitative features of the sea breeze rather than to estimate its onset time and/or propagation speed.

At 1500 UTC 7 June (Fig. 2a), a distinct line of clouds associated with the east coast sea breeze extends from Jacksonville (JAX) down to the southern tip of the state. A similar line of clouds associated with the west coast

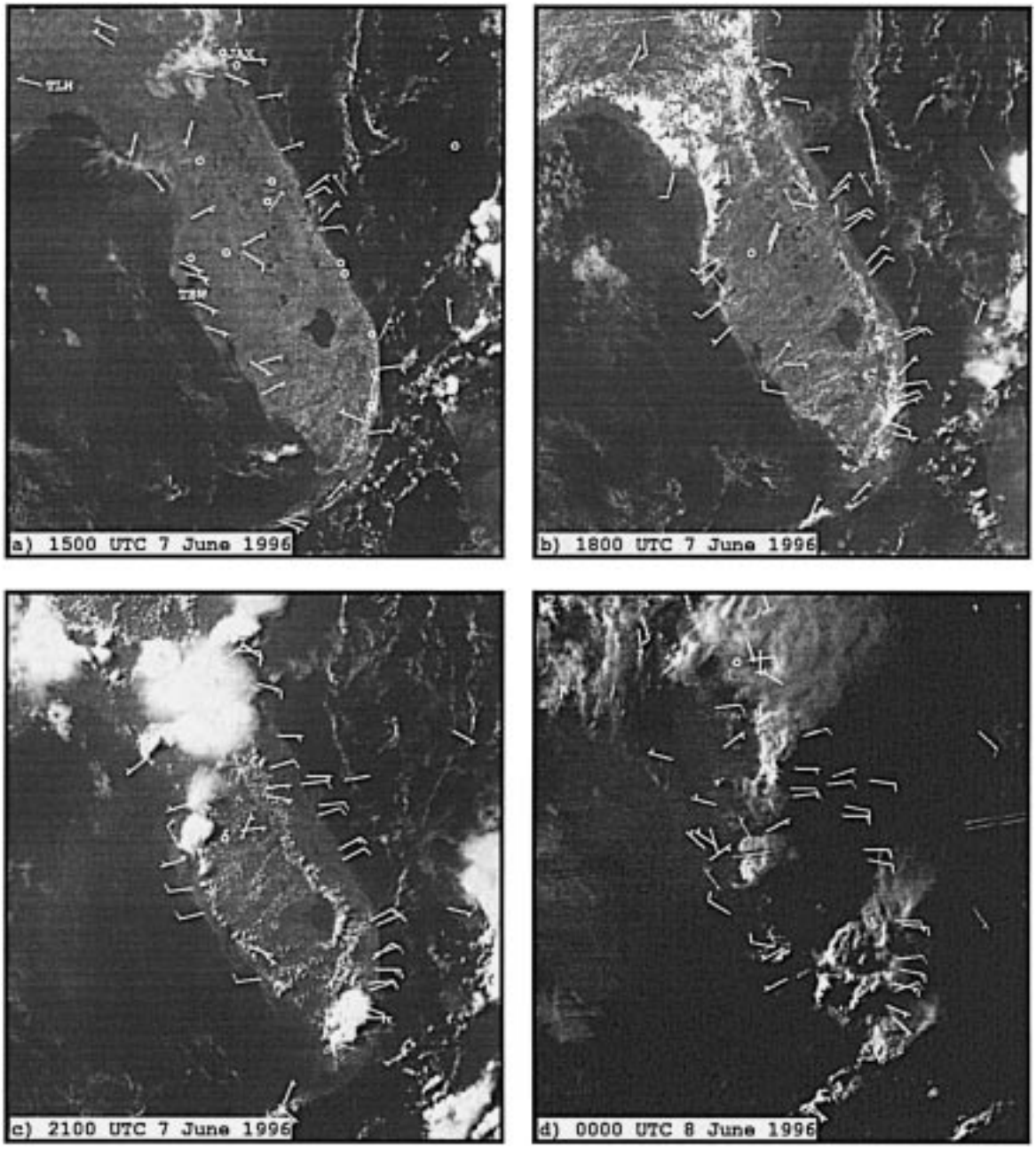

FIG. 2. The 1-km GOES visible imagery and observed surface winds from standard land and buoy sites at (a) 1500 UTC 7 Jun 1996, (b) 1800 UTC 7 Jun 1996, (c) 2100 UTC 7 Jun 1996, and (d) 0000 UTC 8 June 1996. Station identifiers for Jacksonville, FL (JAX), Tampa Bay, FL (TBW), and Tallahassee, FL (TLH) are shown in (a). For surface winds, short barbs = 2.5 m s^{-1}, long barbs = 5 m s^{-1}, and open circles denote calm wind.

sea breeze is just beginning to form at 1500 UTC in the area northwest of TBW and south of Tallahassee. The further development and movement of the west coast sea breeze is clearly evident at 1800 UTC 7 June as the wind direction shifts from offshore (east-southeasterly) to onshore (southwesterly) at most stations along the west coast (Fig. 2b). By 2100 UTC 7 June (Fig. 2c), the east and west coast sea-breeze circulations propagate toward the center of the state. The east and west coast sea breezes are still readily apparent at 0000 UTC 8 June as shown by the visible satellite imagery and surface observations in Fig. 2d. As is common during the warm season afternoons in Florida, significant deep convection is occurring along sections of the sea breeze as early as 1800 UTC.

In the southern half of the Florida peninsula, the sea

breeze penetrates farther inland along the east coast versus the west coast by 2100 UTC (Fig. 2c). This asymmetry in inland penetration of the sea breeze is directly related to the prevailing synoptic flow as shown in previous studies by Estoque (1962), Pielke (1974), and Atkins and Wakimoto (1997). The large-scale flow on 7 June 1996 in the lower troposphere is generally from the east-northeast across the peninsula except along the northwest coast (Fig. 1). With a prevailing onshore (offshore) synoptic flow along the east (west) coast, the sea breeze would be expected to penetrate farther inland on the east versus west coast (Figs. 2b,c).

2) THE 29-KM ETA MODEL FORECAST OF SEA-BREEZE STRUCTURE

The 29-km Eta Model run beginning 0300 UTC 7 June is used to depict the typical evolution of the forecast sea breeze during the 1996 warm season. The Meso Eta Model depicts strong differential heating across the land–sea boundaries along the east and west coasts of Florida as temperatures are forecast to increase more rapidly over land than over water. The evolution of the forecast 2-m temperature gradient is shown by the shading in Figs. 3a–d with darker shading indicating stronger temperature gradients. Note that shaded temperature gradients are shown in Fig. 3 because they provide a more remarkable delineation of land–sea temperature contrasts than isotherms.

For the purposes of qualitative verification of the land–sea temperature contrast, Table 1 lists the observed and forecast temperature at Orlando International Airport (MCO) and at buoy 41009 located approximately 50 km east of CCAS (see Fig. 1 for station locations). The forecast temperature gradient along the east coast is most pronounced around 2100 UTC 7 June (Fig. 3c) when the observed temperature difference of 6.6°C between MCO and 41009 is largest (Table 1). Note that the forecast temperature difference of 4.8°C between MCO and 41009 is also maximized at 2100 UTC although the model underestimates the magnitude of the temperature difference between these stations at all times shown in Table 1.

In conjunction with the developing temperature gradients shown in Fig. 3, the Meso Eta forecasts a transition in the 10-m wind field that is consistent with the onset of the observed sea breeze along Florida's east and west coast. Between 1200 and 1500 UTC 7 June 1996, the forecast winds along Florida's north-central east coast shift from an offshore direction (not shown) to a north-northeasterly onshore direction (Fig. 3e) although forecast winds are more northeasterly than observed at 1500 UTC (Fig. 2a). The forecast 10-m winds continue to veer from north-northeast at 1500 UTC 7 June to east by 0000 UTC 8 June, especially along the northern section of the east coast (Figs. 3e–h) in agreement with the observed wind directions shown in Fig. 2. A more dramatic shift in wind direction occurs along the west coast where weak east-southeast winds at 1500 UTC 7 June veer by more than 250° and become west-northwesterly by 0000 UTC 8 June as the model forecasts a west coast sea breeze (Figs. 3e–h). These changes in forecast wind direction associated with the onset of the west coast sea breeze compare quite well with those shown by the surface observations plotted in Fig. 2.

Atkinson (1981), Clark (1984), and others have shown that the onset of the sea breeze is accompanied by an increase in wind speed. With onshore synoptic flow, there is often no distinct shift in wind direction from offshore to onshore flow but the winds still accelerate as the pressure gradient strengthens in response to stronger heating over land. The changes in wind direction associated with the forecast sea breeze on 7 June 1996 are also accompanied by an increase in wind speed. The 10-m wind speeds (shading in Figs. 3e–h) increase along both coasts especially between 1800 and 2100 UTC 7 June. In fact, there is a marked increase in the 10-m wind speed forecast along the northeast coast as shown by the darker shaded area (speed 5 m s^{-1}) moving from east of the Florida–Georgia border at 1800 UTC to the northeast coast of Florida by 2100 UTC 7 June (Figs. 3f,g). Such changes in 29-km Eta Model 10-m wind speed are useful for identifying the occurrence of forecast sea breezes especially in situations where the prevailing synoptic flow is already onshore.

It is interesting to note that stronger onshore (northeasterly) winds forecast along the northern two-thirds of Florida's east coast at 1500 UTC extend westward toward the center of the peninsula by 2100 UTC (cf. Figs. 3e–g). The forecast matches reasonably well with the inland penetration of the observed east coast sea breeze between 1500 and 2100 UTC as inferred by comparing the location of the cloud lines in Figs. 2a–c. On the other hand, the model does not forecast a shift in wind direction to onshore flow associated with the development of an observed sea breeze along the east and west coast in south Florida (Fig. 2b). The absence of the forecast sea breeze in south Florida likely occurs as the model produces excessive clouds and convective precipitation between 1500 and 1800 UTC in that region thereby limiting the development of the strong temperature gradient, which is prominent in the northern two-thirds of the peninsula (Fig. 3b). Similar deficiencies in forecasting the occurrence of sea breeze were noted for other cases during the 1996 warm season.

Figure 3 shows that the transition to onshore wind flow along both coasts enhances low-level convergence and vertical motion over the middle of the Florida peninsula, which is consistent with the development of a thermally direct circulation. These patterns are illustrated in Fig. 3 by the convergence of the *u* component of the 10-m wind (panels e–h) and the 900-mb vertical velocities (panels a–d). The magnitude of the 10-m zonal wind convergence and negative (upward) 900-mb vertical motions increase markedly from 1500 through 2100 UTC 7 June. Note that the convergence of the

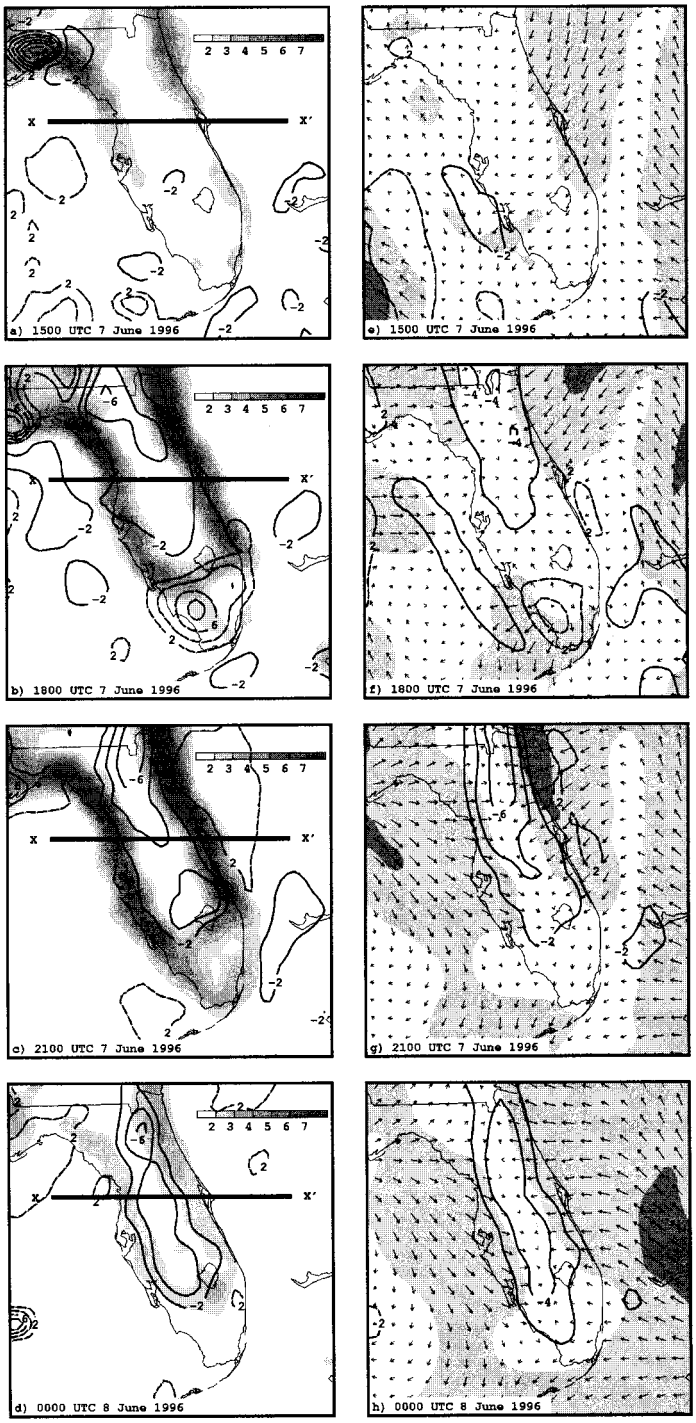

FIG. 3. Evolution of the forecast sea breeze from the 29-km Eta Model run beginning 0300 UTC 7 Jun 1996. (a)–(d) The 2-m temperature gradients (shaded every 1×10^{-2} K km^{-1} as shown by gray scale) and 900-mb vertical velocities (μb s^{-1}); (e)–(h) the 10-m wind speed (shaded every 2.5 m s^{-1}) and direction and divergence of the 10-m wind u component ($\times 10^{-5}$). Charts are shown at 3-h intervals from 1500 UTC 7 June through 0000 UTC 8 Jun. Solid (dashed) lines in (a)–(d) indicate upward (downward) motion with an isopleth interval of 2 μb s^{-1}. Solid (dashed) lines in (e)–(h) indicate convergence (divergence) with an isopleth interval of 2×10^{-5} s^{-1}. Lines X–X' depict the location of vertical cross sections shown in Fig. 4. Note that the zero isopleth is omitted in all panels.

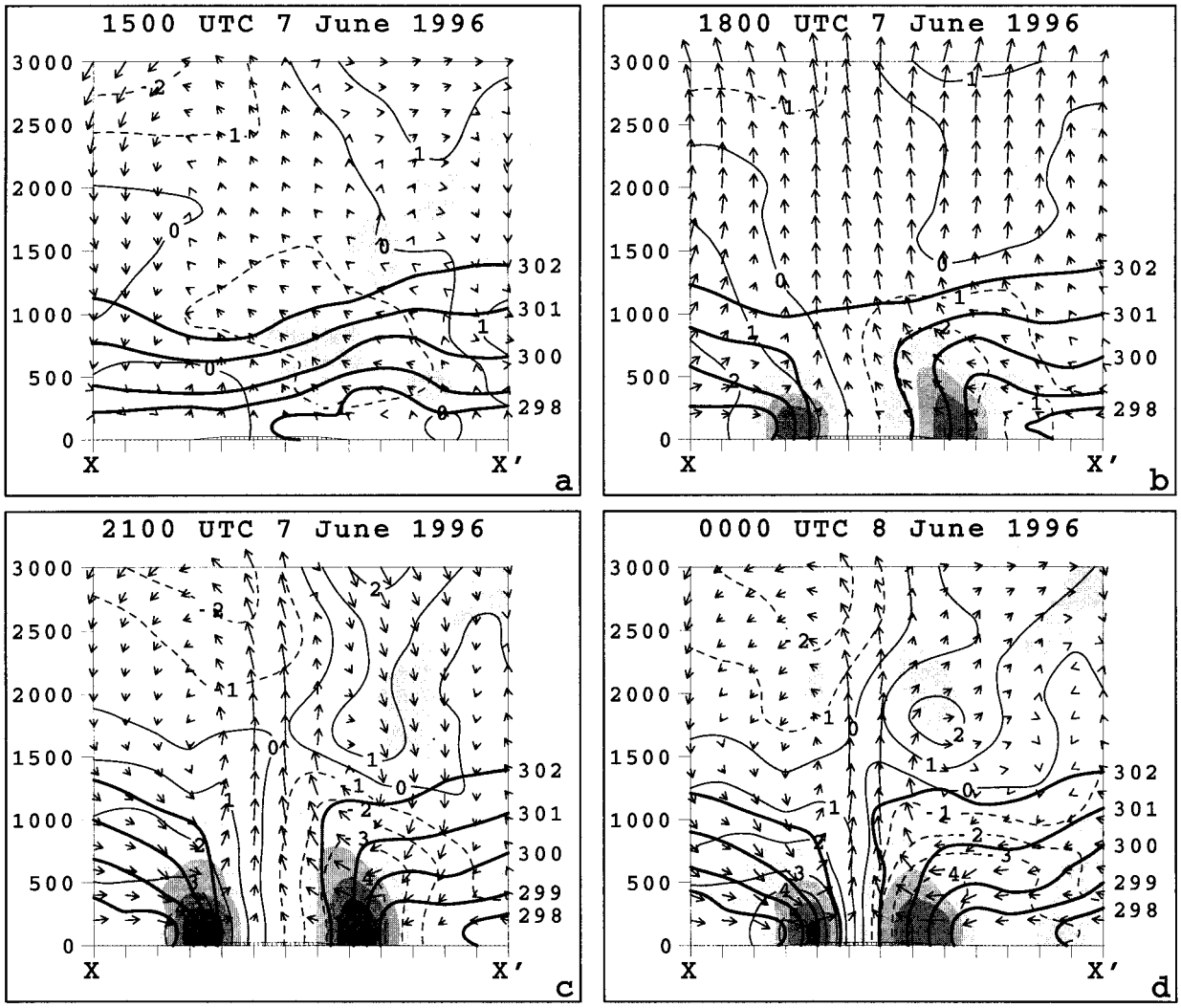

FIG. 4. Vertical cross sections of potential temperature (K), wind tangential to the cross section (m s^{-1}), temperature gradient (10^{-2} K km^{-1}), and circulation along lines X–X' in Fig. 3. Potential temperature (K) is shown by the thick solid lines while shading shows the horizontal temperature gradient at each level. Positive or west (negative or east) tangential winds are indicated by thin solid (dashed) lines. The mean tangential wind at each level is subtracted out from the tangential wind at each point in the plane of the cross sections. Arrows depict circulation in the plane of the cross section. The thin vertical hatched area at the bottom of each cross section approximates the location of land along the lines X–X'. The isopleth interval is 1 K for potential temperature and 1 m s^{-1} for wind speed. Cross sections are plotted as a function of height (m).

zonal wind (u) rather than total wind is used in order to highlight convergent flows, which result from changes in wind speed and direction perpendicular to the coastlines.

The vertical cross sections along the lines X–X' in Figs. 4a–d further illustrate the horizontal scale and vertical extent of thermally direct circulation forecast by the Meso Eta Model on 7 June. It is important to note that the mean tangential wind velocity at each level has been subtracted from the tangential wind shown in Fig. 4 following Atkins and Wakimoto (1997). This technique is very useful to isolate the sea-breeze circulation especially when an east or west coast sea breeze forms in a prevailing onshore flow.

The potential temperatures (K) and shading in Fig. 4 show that the 29-km Eta Model forecasts strong horizontal temperature gradients below 1 km along both coasts, which are maximized around 2100 UTC 7 June. The circulation vectors imply low-level convergence especially along the west coast as the winds below 1 km shift from offshore to onshore by 1800 UTC 7 June. The isotachs of wind speed tangential to the plane of the cross section depict onshore flow along the east coast of Florida exceeding -4 m s^{-1} between 0.25 and 0.5 km at 0000 UTC 8 June (Fig. 4d). Weaker offshore winds on the order of 2 m s^{-1} between 1.5 and 2.0 km above the onshore flow represent the return branch of the thermally direct circulation associated with the fore-

cast east coast sea breeze. A thermally direct circulation associated with the forecast west coast sea breeze is also shown by the onshore (positive) winds at low levels and offshore (negative) winds above 1.75 km near the left side of the cross sections in Figs. 4c,d.

The thermally direct circulation depicted in Fig. 4 extends through the lowest 3 km of the model-simulated atmosphere. The vertical extent of the forecast sea breeze in the Meso Eta Model is significantly higher than the 1–2 km observed at different midlatitude and tropical locations around the world (Atkinson 1981, 144–145). However, dual-Doppler measurements from the Convection and Precipitation/Electrification Experiment on 12 August 1991 found a return (offshore) flow associated with an east coast sea breeze extending above 2 km (Atkins and Wakimoto 1997). Presently, the KSC/CCAS network of 915-MHz Doppler radar wind profilers can be used for verifying the vertical extent of the sea breeze along the central east coast of Florida. However, the 915-MHz profiler data were not available until well after the 1996 warm season evaluation period ended. As a result, these data were not used to compare the depth of the observed and forecast east coast sea breezes.

b. Warm season statistics

The case example from 7 June 1996 demonstrates that the 29-km Eta Model can forecast a sea breeze that is characterized by a thermally direct circulation and changes in low-level horizontal wind speed and direction along either coast. In order to overcome limitations in examining one case and provide greater added value for model users and developers, it is important to quantify how often the model correctly forecasts the occurrence of the Florida sea breeze. Therefore, the following analysis focuses on determining the skill of the Meso Eta Model in forecasting the occurrence of an east or west coast sea breeze anywhere along the Florida peninsula during the entire warm season (May–August 1996). Since there are a number of warm season cases when the model forecasts only an east or west coast sea breeze, the analysis considers separate verification of east and west coast events.

The initial step in the sea-breeze verification is to count the occurrence of forecast and observed east and west coast sea breezes. The verification is performed for all days during the warm season when 1) both observations and 29-km Eta Model forecasts are available and 2) either the east or west coast of Florida is not affected by disturbed weather such as tropical waves, tropical cyclones, or fronts.

The occurrence of observed sea breezes is determined subjectively using the GOES visible imagery and standard surface METAR and buoy observations as shown in Fig. 2. In particular, the visible satellite images at 1-h intervals from 1200 through 2300 UTC are animated to determine if narrow cloud bands similar to those shown in Fig. 2 form along either coast during the 11-h verification period. In addition, the surface data are used to detect shifts in wind direction from onshore to offshore flow and/or increases in wind speed associated with the onset of the sea breeze.

Alternatively, it is possible to use WSR-88D radar data to detect thin lines in reflectivity associated with observed sea breezes as demonstrated by Weckwerth et al (1997) and Atkins and Wakimoto (1997). However, it would be necessary to obtain, process, and examine data for the entire warm season from WSR-88D sites at Jacksonville, Tampa, Melbourne, Miami, Tallahassee, and Key West, Florida, in order to identify the occurrence of east and west coast sea breezes along any portion of the peninsula. In terms of time and resources, such extensive radar data analysis is beyond the scope of the present study.

The occurrence of forecast sea breezes is determined by animating Meso Eta gridded fields similar to those shown in Figs. 3 and 4 at 3-h intervals from all available 0300 UTC model runs. For the purpose of verification, a forecast east or west coast sea breeze is identified when the sequence of 3-h model output shows a shift in wind direction from offshore to onshore flow and/or an increase in wind speed along either coast in combination with the other thermodynamic and kinematic features that appear in Figs. 3 and 4. The mean tangential wind velocity at each level in the cross sections is subtracted from the tangential wind at each point to highlight the sea-breeze circulation. This technique is very important for identifying and isolating thermally direct circulations associated with forecast sea breezes (as shown in Fig. 4) that may not be readily apparent especially with large-scale onshore flow. In conjunction with the gridded model fields, the point or station forecasts at XMR and TBW are also used to help detect changes in wind speed and direction associated with the onset of forecast sea breeze along the east and west coast, respectively.

The occurrence of forecast and observed east and west coast sea breezes as determined from available warm season data are counted and entered in a four-cell contingency table. The data from the contingency table are then used to compute the bias, false alarm rate (FAR), probability of detection (POD), critical success index (CSI), and Heidke skill score (HSS) for east and west coast sea-breeze events. The definitions of the bias, FAR, POD, CSI, and HSS follow Schaefer (1990) and Doswell et al. (1990).

The number of forecast and observed east and west coast sea-breeze events and summary statistics are presented in Table 2. Note that the bias = POD = CSI for both east and west coast verification because there are no occurrences of forecast but not observed sea breezes as shown in Table 2. The number of verification days ($N = 68$) is less than the total number of days (123) during the warm season evaluation period as a result of missing forecast and/or observational data or the presence of disturbed weather. The bias of 0.73 and POD of 0.73 for east coast events reveals that the Meso Eta

TABLE 2. East and west coast sea-breeze events and summary statistics.

	Observed						
	Yes	No	Bias	FAR	POD	CSI	HSS
East coast sea breeze events			0.73	0.0	0.73	0.73	0.65
Forecast							
Yes	33	0					
No	12	23					
West coast sea breeze events			0.67	0.0	0.67	0.67	0.60
Forecast							
Yes	29	0					
No	14	25					

Model forecasts the occurrence of the east coast sea breeze just slightly less than 75% of the time it is observed. The bias of 0.67 and POD of 0.67 is slightly smaller for west coast than for east coast events and indicates that the model also underestimates the occurrence of the west coast sea breeze. The forecast accuracy for east and west coast sea breezes is also reflected by the CSI and HSS. For random forecasts the HSS is equal to zero. Therefore, although slightly more accurate along the east coast, the model does provide an improved guidance over random forecasts for the occurrence of sea breezes along both coasts. Finally, the FAR of 0.0 suggests that the model does not forecast east or west coast sea breezes that are not observed.

There are likely a number of reasons why the 29-km Eta Model correctly forecasts slightly less than 75% of observed east and west coast sea breeze events along the Florida peninsula. One possible explanation, which is based on experience from the AMU warm season forecast exercises, is that the model typically does not forecast the occurrence of observed sea breezes on days characterized by larger-scale forecast errors over a significant portion of Florida. Typical Meso Eta forecast errors noted during the warm season evaluation period relate to the formation of excessive clouds and precipitation too early in the forecast period (mentioned for the 7 June case) and to the propagation of tropical waves and other smaller-scale vortices. For example, the model run beginning at 0300 UTC 18 June 1996 forecasts Tropical Storm Arthur in the western Atlantic to make landfall north of Daytona Beach, Florida. However, Arthur tracked more northwesterly and made landfall in South Carolina while observed sea breezes formed along the east and west coasts of Florida. As a result, the forecast is dominated by the circulation associated with Arthur rather than the characteristic patterns of forecast sea breezes shown in Figs. 3 and 4.

4. Thunderstorm verification

Warm season thunderstorms in Florida result primarily from interactions between mesoscale phenomena. Because models commonly used in operations (i.e., NGM, 48-km Eta) cannot resolve the spatial and temporal details of these phenomena, forecasters must utilize observations and persistence to develop accurate short-term ($<$6 h) thunderstorm forecasts. Given its 29-km gridpoint resolution, the Meso Eta model is not expected to resolve features such as individual convective cells or thunderstorm outflow boundaries. Although thunderstorms are not explicitly forecast by the model, basic diagnostic quantities from its 3-h gridded (1-h point) output provide utility by allowing users to follow trends and make inferences about the environments that may be conducive for thunderstorm development.

The case examples presented by Manobianco and Nutter (1997) demonstrate that the Meso Eta Model occasionally has utility in forecasting convective precipitation over Florida by correctly depicting several environmental features important for thunderstorm development. These features include surface temperature gradients associated with heating in clear versus cloudy areas and low-level wind convergence associated with a developing thermal trough. Precipitation is a measurable response to the wide variety of mesoscale interactions that often lead to the formation of thunderstorms. Therefore, forecast and observed precipitation patterns are compared throughout the 1996 warm season to help quantify the model's added value in forecasting thunderstorms over regions of the Florida peninsula. It should be noted that throughout the remainder of this section, terminology for thunderstorms, convection, and precipitation are used interchangeably.

a. Methodology

The methodology used in this study for the verification of precipitation occurrence differs from traditional methods. The traditional methods used to verify precipitation involve a point-by-point comparison of forecast and observed amounts at selected thresholds over the model grid (e.g., Olson et al. 1995). The statistics such as bias, FAR, POD, and threat score or critical success index derived from such analyses do not usually account for spatial errors in forecasting precipitation. On the other hand, these methods often verify forecast and observed precipitation over periods of 12 to 24 h, which allows for significant errors in forecasting the temporal evolution of precipitation.

The technique used in this study focuses on the occurrence of precipitation ($>$0.25 mm) anywhere within a region on the order of 100 km $\times$ 200 km. Experience from the warm season forecast exercises suggests that broad areas of model-generated precipitation could be subjectively correlated with precipitation that was observed over much smaller sections of the same area. By performing a zone assessment of forecast and observed precipitation occurrence, a far less stringent test of model capabilities is applied than traditional methods that measure exact spatial correlation between forecast and

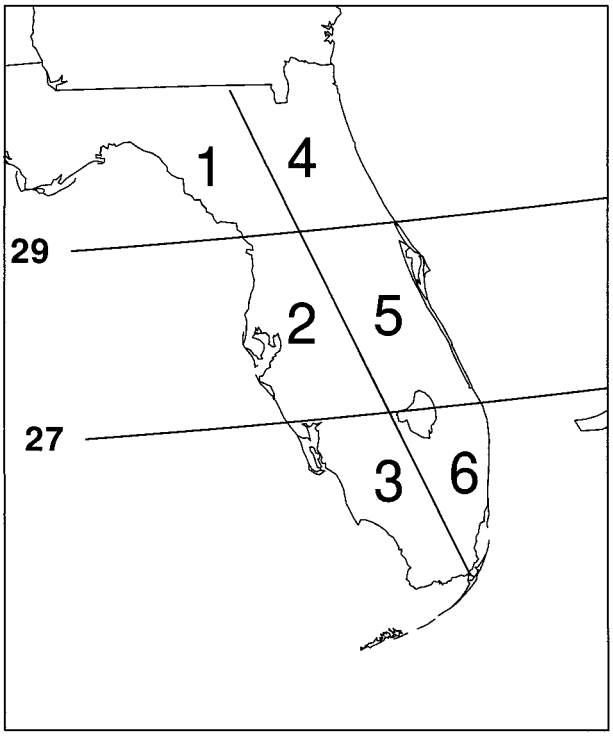

FIG. 5. Map of Florida showing definition of precipitation verification zones.

observed precipitation. However, precipitation forecasts in the current evaluation are verified over 3-h periods to highlight temporal errors and determine whether the model can forecast the observed diurnal cycle in warm season precipitation over Florida. In this regard, the evaluation strategy is more stringent than that used in traditional methods especially when precipitation is verified over much longer time periods (e.g., 24 h).

There are several steps involved in verifying the occurrence of forecast precipitation. First, the state is divided into six verification zones shown in Fig. 5. The motivation for bisecting the state from north to south is to determine if the Meso Eta Model could forecast distinct areas of convection associated with the model's east and/or west coast Florida sea breezes. The remaining divisions along the 27° and 29° latitude lines are subjective and yield six zones of roughly equal area (not counting the westernmost area of the panhandle). Notably, the width of each zone over land is approximately 120 km. Since the 29-km Eta Model cannot resolve features with wavelengths less than $4\Delta x$ or 116 km, the zone width corresponds well with the model's smallest resolvable wavelength.

The next step in the precipitation verification is to count the occurrence of forecast and observed precipitation over land in each zone during 3-h periods from 1500 to 1800 UTC, 1800 to 2100 UTC, and 2100 to 0000 UTC. These time periods are chosen to verify the forecast occurrence of thunderstorms during the 9-h period from 1500 to 0000 UTC (1100 to 2000 EDT) when convection is most often observed in Florida during the warm season. The occurrence of forecast thunderstorms is determined using Meso Eta gridded fields of 3-h accumulated total precipitation and is based on total precipitation values exceeding 0.25 mm anywhere in a zone during the 3-h period. Experience from the warm season forecast exercises suggests that more than 95% of the total precipitation over Florida is generated by the model's convective parameterization. The verification of forecast precipitation occurrence is determined using only gridded data from the 0300 UTC initialization of the model since the gridded data from the 1500 UTC cycle were not available before 1800 UTC.

The occurrence of observed thunderstorms is determined subjectively from all available 4-km visible (VIS) and IR GOES satellite data and from surface weather reports of rain and thunderstorms. The VIS and IR satellite images at every hour from 1500 to 0000 UTC are animated to locate distinct thunderstorm anvils in the VIS data and strong gradients of cold cloud-top temperatures in the IR data. These features are used as a proxy for the occurrence of precipitation in each zone during the 3-h periods. The occurrence of observed precipitation could have been determined from hourly composites derived by NCEP using available Office of Hydrology rain gauge observations and WSR-88D-derived precipitation (Baldwin and Mitchell 1996). However, NCEP did not begin producing the precipitation composites until late July 1996; therefore, they were not available for the entire warm season evaluation period (May–August 1996). It is also possible to use just WSR-88D data for verifying the occurrence of precipitation within each zone. In order to perform such verification, it would be necessary to process and analyze WSR-88D data from multiple Florida sites, which is beyond the scope of this study.

It is likely that anvil debris, cirrus clouds, or the lack of well-defined anvils or cold cloud tops affect the accuracy of the satellite-based, subjective technique in delineating areas of actual precipitation. Therefore, routine surface observations of precipitation (i.e., rain or thunderstorms) are included to account partly for such deficiencies. It is important to point out that surface weather observations alone probably underestimate the occurrence of precipitation given the nonuniform distribution and relative coarse spacing of the stations. In cases where either satellite or surface data are missing for the entire 3-h period, only the remaining available satellite or surface observations are used to identify observed thunderstorms. When both satellite data and surface observations are available, observed thunderstorms are identified in the 3-h window if either data type indicates their presence based on the criteria discussed above.

The occurrences of all forecast and observed thunderstorms as determined from available warm season data in the six zones over each 3-h period are counted

TABLE 3. Summary statistics for the verification of precipitation occurrence within each of six zones shown in Fig. 5. The definitions of the bias, FAR, POD, CSI, and HSS follow Schaefer (1990) and Doswell et al. (1990).

	1500–1800 UTC	1800–2100 UTC	2100–0000 UTC
Zone 1			
Bias	2.44	0.91	0.98
FAR	0.62	0.20	0.23
POD	0.94	0.73	0.75
HSS	0.52	0.48	0.66
Zone 2			
Bias	2.05	1.05	1.31
FAR	0.60	0.24	0.32
POD	0.81	0.79	0.89
HSS	0.60	0.61	0.78
Zone 3			
Bias	1.74	0.88	1.04
FAR	0.53	0.19	0.21
POD	0.81	0.71	0.82
HSS	0.65	0.64	0.78
Zone 4			
Bias	1.57	0.91	1.28
FAR	0.52	0.31	0.37
POD	0.76	0.63	0.81
HSS	0.48	0.53	0.64
Zone 5			
Bias	1.76	1.00	1.22
FAR	0.52	0.30	0.27
POD	0.84	0.70	0.89
HSS	0.61	0.58	0.73
Zone 6			
Bias	1.69	0.86	1.00
FAR	0.53	0.18	0.27
POD	0.79	0.71	0.73
HSS	0.68	0.66	0.72

and entered in four-cell contingency tables. In cases where forecast or observed precipitation is located on zone boundaries or across adjacent zones, these events count as ''yes'' occurrences for each zone containing the specified area of precipitation. The data from these contingency tables are then used to compute the bias, FAR, POD, and HSS for each zone and time period.

b. Results

Summary statistics for each of the zones are presented in Table 3. When all available data are pooled together the sample size of valid forecast–observed data ranges from 73 to 78 depending on zone number and 3-h verification period. Because sample sizes from each zone are relatively small and not independent, it is difficult to determine if subtle differences between the scores in each zone are statistically significant. The following discussion focuses on scores from zone 5 that covers east-central Florida and includes XMR (Fig. 5).

Within the first 3-h period from 1500 to 1800 UTC, a bias of 1.76 indicates that forecast precipitation occurs 76% more often than actually observed. In later periods, the bias improves to 1.00 between 1800 and 2100 UTC before increasing slightly to 1.22 between 2100 and 0000 UTC. As the bias scores improve, the FAR scores correspondingly decrease. Between 1500 and 1800 UTC, the FAR in zone 5 is 0.52, indicating that the occurrence of precipitation is incorrectly forecast on 52% of valid days. In later periods from 1800 to 2100 UTC and 2100 to 0000 UTC, the FAR (bias) decreases to 0.30 (1.00) and 0.27 (1.22), respectively, implying that the model has more utility in delineating whether precipitation is likely to be observed in a specific zone. Since values of POD in zone 5 are 70%, the model tends to accurately forecast the occurrence of most observed rain events. However, these values must be viewed in context with values of bias and FAR; a high POD is only effective when the corresponding FAR is low and the bias near unity. Since the contingency table includes observed precipitation regardless of whether it can be resolved by the 29-km Eta Model, the POD for all zones and time periods may improve (i.e., approach unity) by verifying forecast and observed precipitation only at scales that are resolved by the model.

Examination of the contingency tables used for the analysis (not shown) reveals that precipitation was observed (forecast) in zone 5 on 32% (57%), 51% (51%), and 58% (70%) of valid days during the periods 1500–1800 UTC, 1800–2100 UTC, and 2100–0000 UTC, respectively. A comparison of these percentages indicates that the bias approaches unity during the last two time periods largely due to increases in the frequency of observed precipitation. In general, the 0300 UTC initialization of the Meso Eta Model forecasts precipitation too frequently during the first 3-h period from 1500 to 1800 UTC (1100–1400 EDT). These results are supported by the HSS, which indicates that the model provides the greatest improvement over random forecasts (i.e., HSS = 0) in the later time period from 2100 to 0000 UTC. While this discussion only focuses on scores for zone 5, Table 3 shows similar results for the other zones. Although beyond the scope of the present study, a useful extension of this analysis would be to verify precipitation forecasts for all 3-h time periods from both 0300 and 1500 UTC model runs over the warm and cool season (October 1996–January 1997).

5. Cold front verification

Fronts are usually identified as a line of confluent winds that precede narrow zones of tight gradients in temperature and/or dewpoint temperature (Wallace and Hobbs 1977). Cold fronts in particular represent the leading edge of a transition zone to a relatively colder, drier air mass. A review of theoretical and observational studies on fronts is provided by Bluestein (1986), Keyser (1986), and Carlson (1991). While mesoscale sea-breeze fronts are common during the warm season in Florida, synoptic-scale cold fronts are frequent during the cool season. When these cold fronts pass through central Florida, they are commonly associated with lo-

cally adverse weather that may include extensive precipitation, low visibility, strong horizontal and vertical wind shear, and cold temperatures. Moreover, the environment associated with synoptic-scale cold fronts contains instabilities that are conducive for the intensification of mesoscale weather phenomena (Keyser 1986). Given these possibilities, Meso Eta forecasts of synoptic-scale cold frontal passages through east-central Florida (hereafter referred to as fronts, or cold fronts) are compared with observations for the cool season period October 1996 through January 1997. A single case example is presented that considers some aspects of the Meso Eta Model's capabilities and limitations in depicting small-scale details of cold frontal passages. Finally, a summary is provided that compares the observed and forecast timing of frontal passages at XMR throughout the cool season evaluation period.

a. Case example

The example presented here is an analysis of a forecast and observed cold frontal passage through central Florida on 8–9 November 1996. The Meso Eta forecast for this case is from the 0300 UTC cycle on 8 November 1996 with frontal passage at XMR occurring later that day near 2200 UTC. It is important to point out that this case represents only one example of a cold frontal passage through XMR when the front and precipitation are nearly collocated. In many instances, the maximum precipitation associated with cold fronts passing through central Florida occurs in the warm sector well ahead of the main frontal boundary.

Animation of diagnostic quantities for the Meso Eta forecast grids such as vorticity, vertical velocity, convergence, moisture and temperature advection, convective parameters, etc. provides useful ways to depict the forecast evolution of the atmosphere. Unfortunately, the sparsity of observational data limits verification of these forecasts, particularly over offshore areas to the west and east of the Florida peninsula. Use of the KSC/CCAS mesonet data for verification of this case is not appropriate because the width of the transition zone associated with the forecast synoptic-scale cold front is larger than the area covered by the mesonet. For these reasons, only general, subjective comparisons between the forecast and observations are made in terms of cloud cover, precipitation, low-level winds and dewpoint temperatures, and upper-air and surface data at XMR.

1) CLOUDS AND PRECIPITATION

On 8 November 1996, a surface cold front associated with a developing cyclone was oriented generally in a northeast to southwest direction and extended through North and South Carolina, Georgia, and northern Florida. As the front traversed through central Florida, forecast total cloud fraction and 3-h total precipitation amounts are compared with 4-km IR satellite imagery and observed precipitation composites (Fig. 6). Model forecast cloud fraction depicts the percentage of cloudy area in a grid box and is estimated using relative humidity within all model layers (Zhao et al. 1997). The precipitation amounts shown in Fig. 6 are derived by summing the hourly NCEP composite amounts (Baldwin and Mitchell 1996) over the 3-h forecast period.

At 1800 UTC 8 November, the model depicts a northeast–southwest-oriented band of clouds approximately 500 km wide moving across the Florida peninsula (Fig. 6a). Cloud fractions of 100% are forecast to exist in a narrow band from around JAX to TBW and southwest into the Gulf of Mexico. In comparison, 4-km IR imagery (Fig. 6b) reveals that observed clouds cover approximately the same area as depicted by the forecast cloud cover. In particular, scattered cloud cover is observed over south Florida and over most areas of the Atlantic where forecast cloud fractions are generally less than 70%. Observed clouds appear more dense in the satellite imagery along the same line where the model predicts 100% cloud fractions.

The area of clouds and precipitation associated with this cold front continued to move to the southeast through 0000 UTC 9 November (Figs. 6c–f). While observed 3-h rainfall amounts between 1800 and 2100 UTC locally exceed 6.35 mm across central Florida (Fig. 6d), 2-h accumulations in the same area reach just 2.54 mm between 2100 and 0000 UTC (Fig. 6f). Meanwhile, a new band of heavy precipitation formed offshore over the Atlantic with 2-h rainfall amounts in excess of 25.4 mm (Fig. 6f). As is consistent with all previous case examples, the Meso Eta Model is not capable of resolving the small-scale details of these changes in the cold frontal rainband structure. However, the model does predict a general decrease in precipitation amounts across central Florida with a corresponding split in the primary cold frontal rainband (Fig. 6e).

2) WINDS AND DEWPOINT TEMPERATURES

While the animation of cloud cover and precipitation forecasts are useful for identifying the extent and motion of weather associated with cold frontal passages, surface data are required to track the position of the cold front. The parameters used to identify the position of the frontal zone near the surface usually include winds, pressure (heights), moisture, or temperature. As pointed out by Wallace and Hobbs (1977, 118), dewpoint gradients rather than temperature gradients are often more reliable to indicate the position of fronts. In this case, winds and dewpoint temperature gradients provide the strongest representation of frontal position at 2100 UTC 8 November (Fig. 7).

For this example, a line of confluent winds appears in the forecast streamlines to the east of the Florida peninsula (Fig. 7). This line precedes the leading edge of rapidly decreasing forecast dewpoint temperatures across central Florida (shading in Fig. 7). Observations

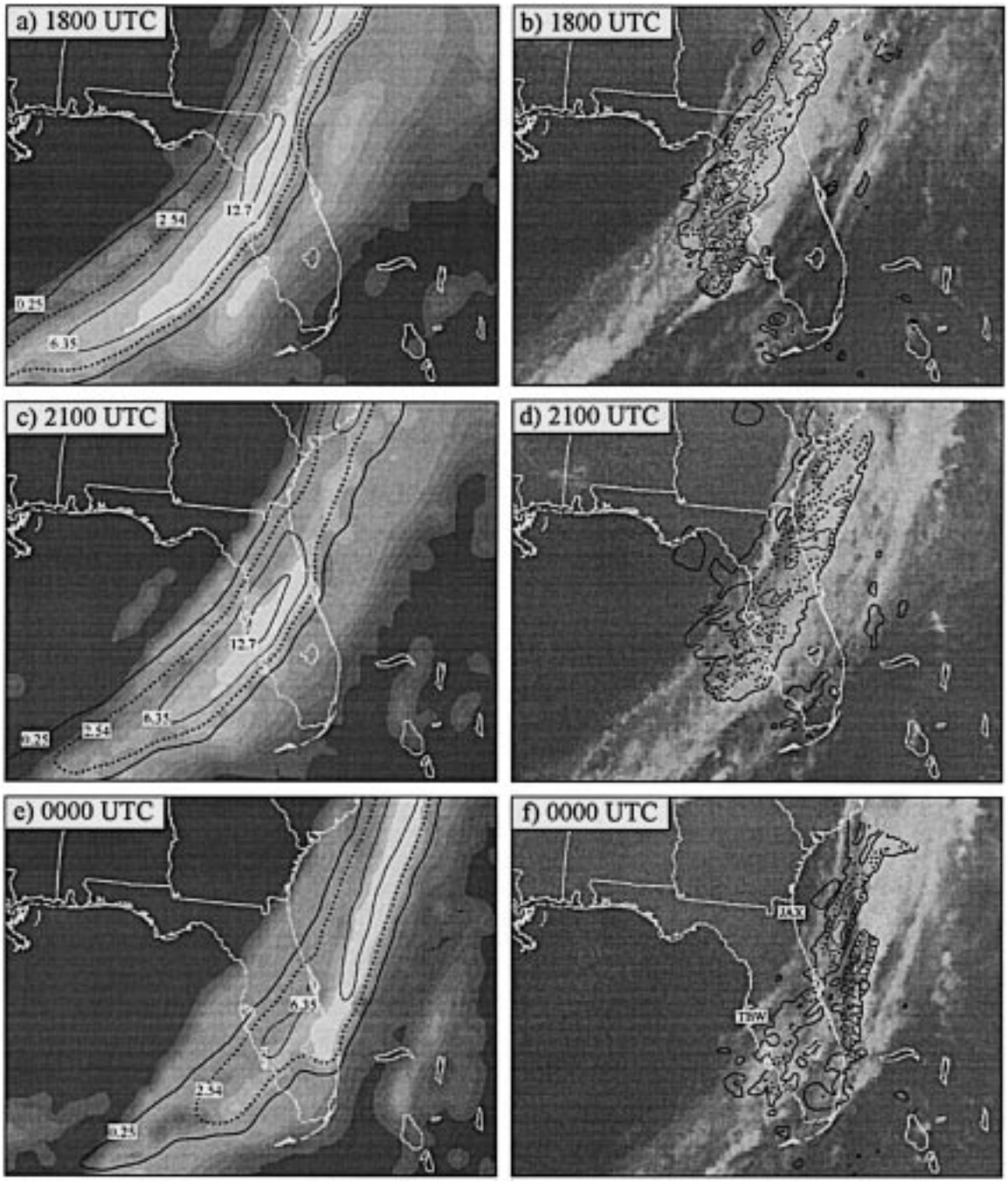

FIG. 6. Forecast total cloud fraction and 3-h precipitation in (a), (c), and (e) with corresponding 4-km GOES IR imagery and estimates of observed 3-h precipitation in (b), (d), and (f). Charts are shown at 3-h intervals from 1800 UTC 8 Nov through 0000 UTC 9 Nov as labeled in each panel. Forecast total cloud fraction is shaded from 0% (darkest) to 100% (lightest) at intervals of 10%. The 3-h forecast and observed precipitation is accumulated from 1500 to 1800 UTC, 1800 to 2100 UTC, and 2100 to 0000 UTC with isopleth intervals at 0.25, 2.54 (dashed), 6.35, 12.7, 19.05, and 25.4 mm. (f) Observed precipitation is accumulated for 2 h due to missing data at 2200 UTC. JAX and TBW are shown in (f).

of wind and dewpoint temperature plotted in the figure agree reasonably well with these forecast parameters. In particular, wind directions generally match those indicated by the forecast streamlines although discrepancies exist especially along Florida's southeastern coast. Observed dewpoint temperatures are within about $\pm 2^{\circ}$C of forecast values and clearly indicate a sharp decrease to the northwest across central Florida. At 2100 UTC, the leading edge of both the observed and forecast frontal zones are analyzed to be nearly collocated as

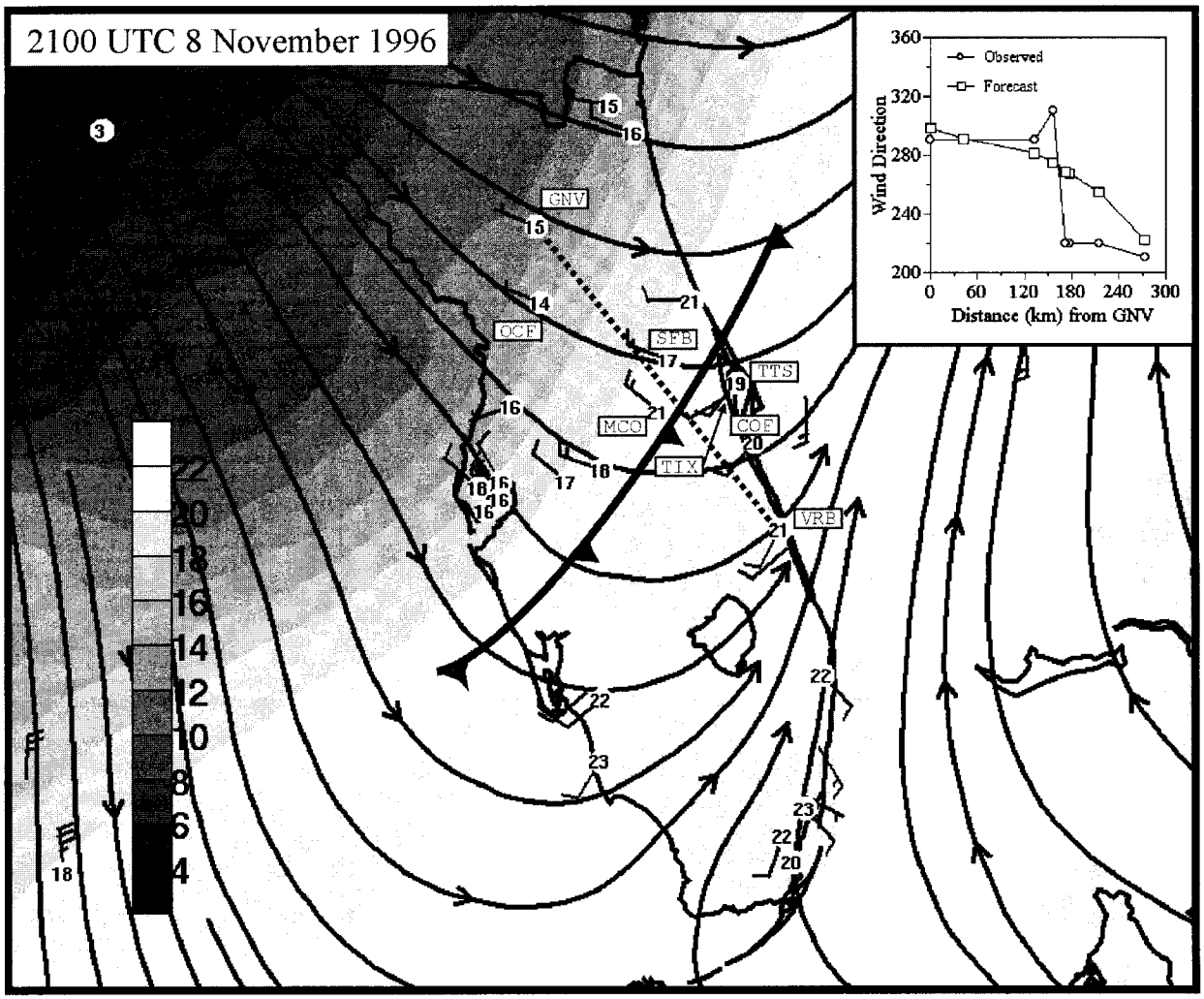

FIG. 7. Forecast 10-m wind streamlines and 1000-mb dewpoint temperatures (°C) with available observations of wind (m s^{-1}) and dewpoint temperatures (°C) at 2100 UTC 8 Nov 1996. Forecast dewpoint temperatures are shown in gray shading every 2°C with darker shading representing drier air as indicated on the temperature scale. Long (short) barbs represent 5 (2.5) m s^{-1} wind observations with numerals shown for dewpoint temperature observations. Inset graph shows observed and forecast wind direction (°) plotted as a function of distance from Gainsville (GNV), along the dotted line between GNV and Vero Beach (VRB). The data points plotted in the graph correspond to station locations along the dotted line at GNV, Ocala (OCF), Sanford (SFB), MCO, shuttle landing facility (TTS), Titusville (TIX), Patrick Air Force Base (COF), and VRB.

shown in Fig. 7. Note that the cold front is shown primarily over land where surface observations are available to define the location of the observed front. The observed front is shown at the leading edge of the transition to lower dewpoint temperature in the region where surface winds back from northwesterly to southwesterly (Fig. 7). The collocated forecast cold front is positioned at the leading edge of the forecast dewpoint temperature gradient.

Close examination of Fig. 7 reveals that there are differences in the horizontal scale of the collocated forecast and observed frontal zones. In particular, the shift in forecast wind direction across the frontal zone is more gradual than observed as demonstrated by the plot of wind direction along a line normal to the front shown in Fig. 7. The forecast winds back from northwest (~290) to southwest (~220) over a distance of roughly 220 km between Ocala (OCF) and Vero Beach (VRB) (Fig. 7). A similar shift in observed wind direction associated with the frontal zone occurs over a much shorter distance on the order of 40 km between MCO and the shuttle landing facility (TTS). Although the model appears to forecast the location of the frontal zone quite accurately across central Florida, the 29-km gridpoint resolution is not adequate to capture the sharpness of the observed cold front.

3) SURFACE POINT FORECASTS AT XMR

It is possible to identify the time when the leading edge of the frontal zone passes through XMR using

hourly surface data. Before using meteograms of hourly surface data to identify frontal passages at a point, it is necessary to note the existence of the approaching front in the horizontal distribution of forecast and/or observed data (i.e., Figs. 6 and 7). When considered alone, time series of surface parameters sometimes exhibit shifts that could be misinterpreted as frontal passages.

Meteograms of forecast and observed temperature, dewpoint temperature, mean sea level pressure (MSLP), wind speed, and wind direction at XMR are shown for the 33-h period from 0300 UTC 8 November through 1200 UTC 9 November 1996 (Fig. 8). At 2200 UTC, observed dewpoint temperatures begin to decrease rapidly at the rate of about 5°C h^{-1} (Fig. 8b). Forecast dewpoint temperatures also begin decreasing at that time, though at a slower rate relative to observations. A sudden shift in observed wind direction (Fig. 8e) is also observed at 2200 UTC. The corresponding forecast wind shift is more gradual, yet clearly evident. The meteograms of dewpoint temperature and wind direction (Figs. 8b,e) indicate that the leading edge of the forecast and observed frontal zone passes through XMR around 2200 UTC 9 November 1996.

Other parameters displayed in the meteograms do not show as clear a depiction of when the front arrives at XMR. For example, forecast and observed temperatures begin to decrease prior to the frontal passage likely in response to the normal diurnal cooling near sunset. It is interesting to note that forecast changes in meteogram parameters occur more slowly than observed. At 2200 UTC, the observed wind direction at XMR shifts from about 210° to 300° in 1 h. The same shift in forecast wind direction occurs gradually over 4 h from about 2000 UTC 8 November to 0000 UTC 9 November. Therefore, hourly meteogram data also indicate that the Meso Eta Model does not resolve the sharp gradients of temperature, moisture, wind, etc. at the scales that are characteristic of observed frontal zones.

4) UPPER-AIR POINT FORECASTS AT XMR

The passage of the cold front through XMR is also apparent in forecast and observed profiles of upper-air temperature, dewpoint temperature, and winds. The forecast and observed soundings at XMR 10 h prior and 14 h after frontal passage are depicted in Figs. 9a and 9b, respectively. The soundings reveal that the model generally is able to handle the increase in moisture as clouds and precipitation enter central Florida and the subsequent drying that occurs after frontal passage. Moreover, the depth of the postfrontal intrusion of cold air is evident by the low-level temperature inversion and wind shifts that develop in the lower 200 mb of both forecast and observed soundings (Fig. 9b).

Many of the differences between the forecast and observed variables shown in Figs. 8 and 9 are consistent with the cool season objective verification of those parameters discussed in NM99. For example, dewpoint temperatures and wind speeds following cold frontal passage are greater than observed (Figs. 8b,d). A similar positive bias appears in the 1996 cool season statistics shown in NM99 (their Figs. 2d,g). The forecast temperature inversion that develops near 700 mb after frontal passage (Fig. 9b) is at a higher level than observed. This result is again consistent with the cool season bias shown in NM99 (their Fig. 5d), which depicts a sharp cool bias at around the same level.

b. Cold frontal timing at XMR

The case example discussed in section 5a demonstrates some of the capabilities and limitations of the Meso Eta Model in forecasting cold frontal passages through central Florida. However, not all forecasts of frontal passages are quite as accurate. Many cases are much more complicated and involve phenomena such as prefrontal rain bands, developing cyclogenesis, and stalled fronts. In an attempt to quantify the overall accuracy of cold front forecasts in central Florida, the timing of cold frontal passages through XMR is documented throughout the cool season period.

To perform a seasonal verification of frontal passages at XMR, all available 0300 UTC forecast grids are examined for the presence of fronts. The 0300 UTC Meso Eta forecasts of MSLP, 10-m winds, 850-mb vertical velocity, 2-m dewpoint temperature, and 1000-mb frontogenesis (Carlson 1991, 351) are all used to help identify the movement of cold fronts across central Florida. Once the frontal passage events are identified, observed and forecast meteograms from 0300 and 1500 UTC model runs similar to those shown in Fig. 8 are used to determine the time of frontal passage to the nearest hour. Results of forecast and observed frontal passages through XMR are summarized in Table 4.

A total of 10 observed fronts passed through XMR during the cool season period on days for which both gridded and point forecast data and observed surface data at XMR are available. Several other cold fronts entered northern Florida, but they are not counted in this summary because observations indicate that the fronts never actually reached XMR. Of the cases considered in Table 4, more than half of the forecast cold fronts passed through XMR within 1 h of the observed frontal passage. For the 0900 UTC 19 December event, the forecast cold front is not evident at the end of the 33-h forecast cycle beginning 0300 UTC 18 December, as indicated by the word ''None'' in Table 4. Overall, timing accuracy does not appear to depend on forecast duration. Model runs initiated at 0300 UTC are slightly more accurate in forecasting cold frontal passage at XMR than those initiated at 1500 UTC. However, this result may be due to the small number of cases sampled during this cool season period.

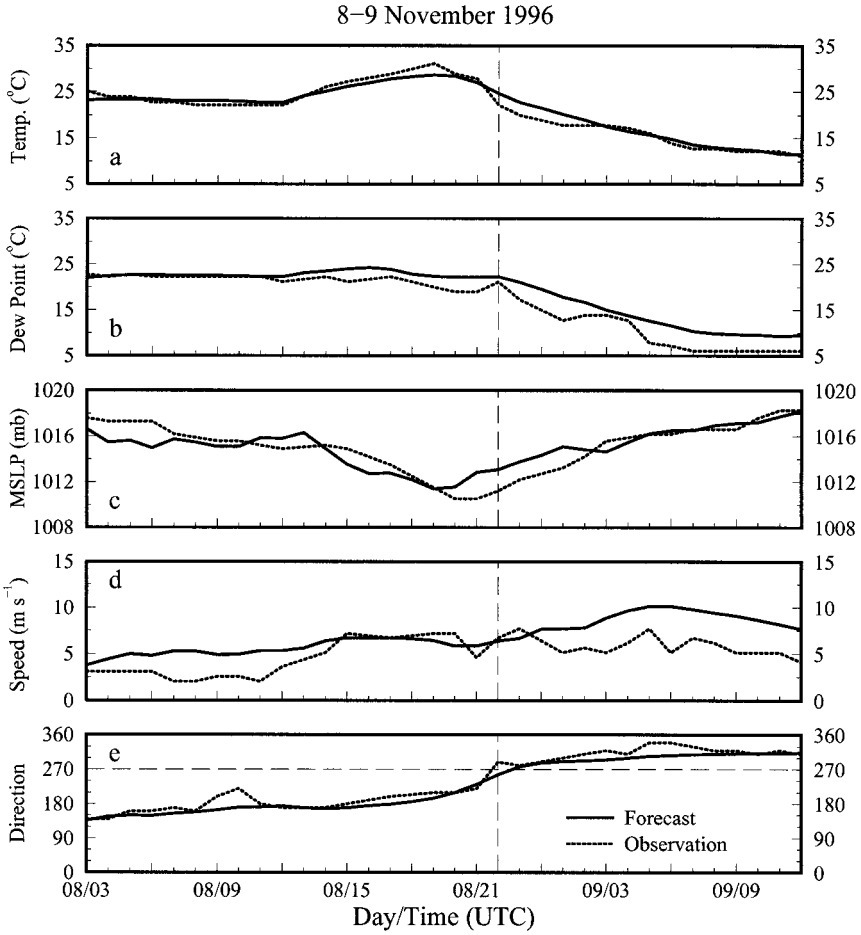

FIG. 8. Forecast and observed meteograms at XMR of (a) 2-m temperature, (b) 2-m dewpoint temperature, (c) MSLP, (d) 10-m wind speed, and (e) 10-m wind direction. The meteograms cover the 33-h period from 0300 UTC 8 Nov through 1200 UTC 9 Nov 1996. Solid lines depict forecast values from the 0300 UTC Meso Eta Model run, dotted lines depict observed values, and the vertical dashed lines indicate the apparent time of frontal passage through XMR at 2200 UTC 8 November. The horizontal dashed line in (e) is added for emphasis of westerly winds.

6. Summary and conclusions

The evaluation described here and in the companion paper (NM99) is designed to assess the utility of the Meso Eta Model for weather forecasting in support of 45WS, SMG, and NWS MLB operational requirements. The objective verification of the model presented in Part I (NM99) focused on the overall accuracy of wind, temperature, and moisture forecasts at XMR, TBW, and EDW for the 1996 and 1997 warm (May–September) and cool (October–January) seasons. The subjective evaluation discussed in this paper includes warm season forecast exercises and phenomenological verification focusing primarily on limited case studies and seasonal evaluations of sea breezes, thunderstorms, and cold fronts. Seasonal verification is very important to quantify the added value of model forecasts for specific phenomena that cannot be readily inferred from statistics over many cases (i.e., from objective verification). A seasonal evaluation is also useful because conclusions drawn about model limitations and capabilities in forecasting selected aspects of sea breezes, thunderstorms, and cold fronts are limited by examining only a few cases.

Results from the subjective evaluation presented in this paper that can be important for operational forecasting include the following.

1) The Meso Eta forecast sea breeze is characterized by a thermally direct circulation that forms in response to differential heating across the land–sea boundaries along the Florida peninsula. The occurrences of east or west coast sea breezes are correctly forecast about 75% of the time they are observed during the warm season. Errors in forecasting the occurrence of the observed sea breeze are often related to larger-scale model errors over a significant portion of the Florida peninsula. Lastly, the 29-km

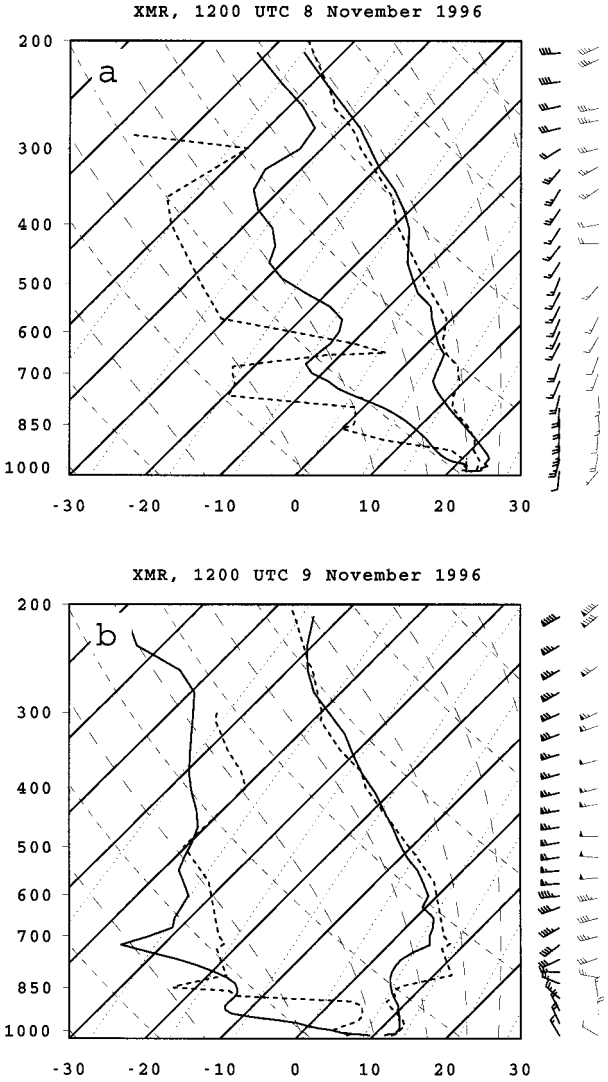

FIG. 9. Skew *T*–log *p* plots of forecast and observed sounding data at XMR valid (a) 1200 UTC 8 Nov 1996 and (b) 1200 UTC 9 Nov. All forecasts are taken from the model run initialized 0300 UTC 8 Nov 1996. Heavy solid (dashed) lines are forecast (observed) temperature and dewpoint temperatures (°C). Forecast (observed) wind barbs (short barb = 2.5 m s^{-1}, long barb = 5 m s^{-1}, flag = 25 m s^{-1}) are shown in bold (normal) to the right of each plot.

gridpoint resolution of the model is not sufficient to resolve the observed horizontal scale of individual circulations associated with the observed west and/or east coast sea breezes.

2) Thunderstorm verification during the 1996 warm season reveals that the Meso Eta Model is capable of predicting areas of organized convection, particularly from 1800 to 2100 UTC and 2100 to 0000 UTC. On the other hand, the model is also subject to subtle errors that can lead to incorrect forecasts of warm season convective precipitation. In particular, the model often generates excessive rainfall during the late morning to early afternoon hours (1500–1800 UTC) and is not capable of forecasting individual thunderstorms. It is important to reiterate that this verification focuses on the occurrence of precipitation in zones on the order of 20 000 km^2 (100 km × 200 km) over 3-h periods. As such, this methodology highlights whether the model can forecast the observed diurnal variations in precipitation over Florida without requiring an exact spatial correlation between forecast and observed precipitation at selected thresholds (i.e., the traditional approach for computing precipitation accuracy statistics like the bias and threat score).
3) During the 1996 cool season, more than half of the 10 forecast cold fronts passed through XMR within 1 h of the observed frontal passage. The spatial and temporal evolution of weather associated with frontal passages is depicted well by the 3-h forecast gridded products. However, the ability of the model to represent small-scale details such as the width of the surface frontal zone is limited by the model's 29-km resolution.

Results from the objective verification in Part I indicate that Meso Eta point forecasts at XMR, TBW, and EDW contain identifiable biases that vary by season and location, but which still provide useful forecast guidance as long as users recognize possible sources for the errors (NM99). On the other hand, results from the subjective verification demonstrate that model forecasts of developing weather events such as thunderstorms, sea breezes, cold fronts, etc. are not always as accurate as might otherwise be implied by the seasonally averaged error statistics. Although the objective statistics do not indicate whether the model provides more accurate forecast guidance on average during either the warm or cool seasons, results from the subjective verification suggest that model forecasts over central Florida may be more *useful* during the cool season. This statement is based on the fact that the Meso Eta Model resolution is not yet sufficient to resolve the small-scale details of sea and river/lake breeze circulations, thunderstorm outflow boundaries, and other phenomena that play a dominant role in determining the short-term evolution of weather over east-central Florida during the warm season. These lessons learned from both portions of the AMU's Meso Eta evaluation should apply equally as well to the recently upgraded ''early'' Eta Model running with a similar 32-km horizontal resolution (Rogers et al. 1997).

In closing, it is worth reiterating that the daily, real-time warm season forecast exercise proved to be a valuable component of the overall subjective verification because it revealed how operational forecasters could use the 0300 UTC cycle of the Meso Eta Model for local forecasting. These exercises showed that animation of 3-h model output with color enhancements and overlay of multiple fields is helpful to identify features and trends that could become important for developing weather. Availability of digital gridded (point) forecasts

TABLE 4. Time of forecast and observed frontal passages (FROPA) through XMR for the 1996–97 cool season evaluation period. Forecast duration indicates the length of the forecast in hours when the forecast front passes through XMR. Timing errors are calculated in hours as observed passage minus forecast passage. In this manner, negative (positive) timing errors indicate that forecast fronts arrived at XMR too late (early). For some days, frontal passages are listed multiple times because the same front is apparent in subsequent model runs.

Observed FROPA at XMR		0300 UTC forecast cycle				1500 UTC forecast cycle			
		FROPA at XMR				FROPA at XMR			
Date	Time (UTC)	Date	Time (UTC)	Duration (h)	Error (h)	Date	Time (UTC)	Duration (h)	Error (h)
19 Oct	0500	19 Oct	0900	30	−4	Not available			
		19 Oct	0600	3	−1				
3 Nov	0200	2 Nov	2300	20	+3	3 Nov	0300	12	−1
8 Nov	2200	8 Nov	2200	19	0	8 Nov	2200	31	0
						8 Nov	2300	8	−1
22 Nov	1200	22 Nov	1300	10	−1	22 Nov	1400	24	−2
26 Nov	1700	26 Nov	1700	14	0	26 Nov	1900	4	−2
2 Dec	0900	2 Dec	0900	30	0	2 Dec	1200	21	−3
		2 Dec	0900	6	0				
8 Dec	1000	8 Dec	0900	6	+1	8 Dec	1200	21	−2
19 Dec	0900	None		30		19 Dec	1300	22	−4
		19 Dec	1000	7	−1				
9 Jan	2300	10 Jan	0200	23	−3	10 Jan	0400	13	−5
16 Jan	1700	16 Jan	1900	16	−2	16 Jan	1800	27	−1
						16 Jan	2300	8	−6

at 3-h (1 h) intervals is important because it gives users the flexibility in display and analysis options while providing the temporal resolution needed to track specific aspects of weather events such as the timing of cold frontal passages. Indeed, experience gained during daily inspection of Meso Eta graphical displays stimulated many internal discussions leading to the development of the mesoscale verification strategies presented here. In order to exploit the four-dimensional capability of the Meso Eta and other models in forecasting possible realizations of the atmosphere, sufficient communication bandwidth and computer processing power are necessary to retrieve, process, and examine output data. This requirement will become more important in the future as NCEP increases the number of Eta Model runs per day, the model resolution, and potentially the frequency of model output.

Acknowledgments. The authors thank Dr. F. Merceret (NASA KSC), Mr. R. Lafosse (SMG), Mr. T. Oram (SMG), and Mr. W. Roeder (45WS) for their comments and suggestions on an earlier version of the manuscript. Two anonymous reviewers offered very useful comments that improved the paper.

REFERENCES

Atkins, N. T., and R. M. Wakimoto, 1997: Influence of the synoptic-scale flow on sea breezes observed during CaPE. *Mon. Wea. Rev.*, **125,** 2112–2130.

Atkinson, B. W., 1981: *Meso-Scale Atmospheric Circulations.* Academic Press, 496 pp.

Baldwin, M., and K. E. Mitchell, 1996: The NCEP hourly multisensor U.S. precipitation analysis. Preprints, *11th Conf. on Numerical Weather Prediction,* Norfolk, VA, Amer. Meteor. Soc., J95–J96.

Black, T. L., 1994: The new NMC mesoscale Eta Model: Description and forecast examples. *Wea. Forecasting,* **9,** 265–278.

Blanchard, D. O., and R. E. Lopez, 1985: Spatial patterns of convection in South Florida. *Mon. Wea. Rev.*, **113,** 1282–1299.

Bluestein, H. B., 1986: Fronts and jet streaks: A theoretical perspective. *Mesoscale Meteorology and Forecasting,* P. Ray, Ed., Amer. Meteor. Soc., 216–258.

Boybeyi, Z., and S. Raman, 1992: A three-dimensional numerical sensitivity study of convection over the Florida peninsula. *Bound.-Layer Meteor.*, **60,** 325–359.

Boyd, B. F., W. P. Roeder, J. B. Lorens, D. S. Hazen, and J. W. Weems, 1995: Weather support to pre-launch operations at the Eastern Range and Kennedy Space Center. Preprints, *Sixth Conf. on Aviation Weather Systems,* Dallas, TX, Amer. Meteor. Soc., 135–140.

Brody, F. C., F. A. Lafosse, D. G. Bellue, and T. D. Oram, 1997: Operations of the National Weather Service Spaceflight Meteorology Group. *Wea. Forecasting,* **12,** 526–544.

Carlson, T. N., 1991: *Mid-Latitude Weather Systems.* Harper-Collins Academic, 507 pp.

CIMSS, cited 1997: GOES-8/9 precipitable water/NCEP Eta comparison. [Available online at http://cimss.ssec.wisc.edu/model/daily/goes8-html.]

Clark, R. H., 1984: Colliding sea breezes and the creation of internal atmospheric bore waves: Two-dimensional numerical studies. *Aust. Meteor. Mag.*, **32,** 207–226.

Cortinas, J. V., Jr., and D. J. Stensrud, 1995: The importance of understanding mesoscale model parameterization schemes for weather forecasting. *Wea. Forecasting,* **10,** 716–740.

Doswell, C. A., R. Davies-Jones, and D. Keller, 1990: On summary measures of skill in rare event forecasting based on contingency tables. *Wea. Forecasting,* **5,** 576–585.

EMC, cited 1998: Environmental Modeling Center: Mesoscale Modeling Branch FAQ. [Available online at http://nic.fb4.noaa.gov:8000/research/FAQ-Eta.html.]

Ernst, J. A., and F. J. Merceret, 1995: The Applied Meteorology Unit: A tri-agency applications development facility supporting the space shuttle. Preprints, *Sixth Conf. on Aviation Weather Systems,* Dallas, TX, Amer. Meteor. Soc., 266–269.

Estoque, M. A., 1962: The sea breeze as a function of prevailing synoptic situation. *J. Atmos. Sci.*, **19,** 244–250.

Friday, E. W., Jr., 1994: The modernization and associated restruc-

turing of the National Weather Service: An overview. *Bull. Amer. Meteor. Soc.,* **75,** 43–52.

Kalnay, E., G. DiMego, S. Lord, H.-L. Pan, M. Iredell, M. Ji, D. B. Rao, and R. Reynolds, 1996: Recent advances in modeling at the National Centers for Environmental Prediction. Preprints, *11th Conf. on Numerical Weather Prediction,* Norfolk, VA, Amer. Meteor. Soc., J3–J8.

Keyser, D., 1986: Atmospheric fronts: An observational perspective. *Mesoscale Meteorology and Forecasting,* Peter Ray, Ed., Amer. Meteor. Soc., 216–258.

Manobianco, J., 1996: Report on the installation and evaluation of the Mesoscale Atmospheric Simulation System. NASA Contractor Rep. CR-201151, 45 pp. [Available from ENSCO, Inc., Applied Meteorology Unit, 1980 N. Atlantic Ave., Cocoa Beach, FL 32931.]

——, and P. A. Nutter, 1997: Evaluation of the 29-km Eta Model for weather support to the United States space program. NASA Contractor Rep. CR-205409, 103 pp. [Available from ENSCO, Inc., Applied Meteorology Unit, 1980 Atlantic Ave., Cocoa Beach, FL 32931.]

——, J. W. Zack, and G. E. Taylor, 1996: Workstation-based real-time mesoscale modeling designed for weather support to operations at the Kennedy Space Center and Cape Canaveral Air Station. *Bull. Amer. Meteor. Soc.,* **77,** 653–672.

Mesinger, F., 1996: Improvements in quantitative precipitation forecasts with the Eta regional model at the National Centers for Environmental Prediction: The 48-km upgrade. *Bull. Amer. Meteor. Soc.,* **77,** 2637–2649.

Nutter, P., and J. Manobianco, 1999: Evaluation of the 29-km Eta Model. Part I: Objective verification at three selected stations. *Wea. Forecasting,* **14,** 5–17.

Olson, D. A., N. W. Junker, and B. Korty, 1995: Evaluation of 33 years of quantitative precipitation forecasting at NMC. *Wea. Forecasting,* **10,** 498–511.

Pielke, R., 1974: A three-dimensional numerical model of the sea breeze over South Florida. *Mon. Wea. Rev.,* **102,** 115–139.

——, and M. Segal, 1986: Mesoscale circulations forced by differential terrain heating. *Mesoscale Meteorology and Forecasting,* P. Ray, Ed., Amer. Meteor. Soc., 516–548.

Priselac, E., J. E. Sardonia, and T. C. Adang, 1997: Operational weather support for NASA space shuttle ferry flights. Preprints, *Seventh Conf. on Aviation Weather Systems,* Long Beach, CA, Amer. Meteor. Soc., 35–39.

Rogers, E., D. G. Deaven, and G. J. DiMego, 1995: The regional analysis system for the operational ''early'' Eta Model: Original 80-km configuration and recent changes. *Wea. Forecasting,* **10,** 810–825.

——, T. L. Black, D. G. Deaven, and G. J. DiMego, 1996: Changes to the operational ''early'' Eta analysis/forecast system at the National Centers for Environmental Prediction. *Wea. Forecasting,* **11,** 391–413.

——, and Coauthors, 1997: Changes to the NCEP operational ''early'' Eta analysis/forecast system. NWS Tech. Procedures Bull. 447, National Oceanic and Atmospheric Administration/National Weather Service, 34 pp. [Available from National Weather Service, Office of Meteorology, 1325 East–West Highway, Silver Spring, MD 20910.]

Schaefer, J. T., 1990: The critical success index as an indicator of warning skill. *Wea. Forecasting,* **5,** 570–575.

Wallace, J. M., and P. V. Hobbs, 1977: *Atmospheric Science—An Introductory Survey.* Academic Press, 467 pp.

Weckwerth, T. M., J. W. Wilson, R. M. Wakimoto, and A. Crook, 1997: Horizontal convective rolls: Determining the environmental conditions supporting their existence and characteristics. *Mon. Wea. Rev.,* **125,** 505–526.

Zhao, Q., T. L. Black, and M. E. Baldwin, 1997: Implementation of the cloud prediction scheme in the Eta Model at NCEP. *Wea. Forecasting,* **12,** 697–712.